Nanocomposites-based Electrochemical Aptasensor for Dimethyl Methylphosphonate (DMMP) Detection

Farah Nabila Diauudin,[1] Siti Aminah Mohd Noor,[2] Jahwarhar Izuan Abdul Rashid,[2] Safura Taufik,[2] Victor Feizal Knight,[3] Wan Md Zin Wan Yunus,[4] Keat Khim Ong,[2] Alinda Samsuri,[2] and Intan Juliana Samsudin[2]

[1]Faculty of Defence Science and Technology, National Defence University of Malaysia, Sungai Besi Camp, 57000 Kuala Lumpur

[2]Centre for Defence Foundation Studies, National Defence University of Malaysia, Sungai Besi Camp, 57000 Kuala Lumpur.

[3]Research Centre for Chemical Defence, National Defence University of Malaysia, Sungai Besi Camp, 57000 Kuala Lumpur.

[4]Centre for Tropical Studies, National Defence University of Malaysia, Sungai Besi Camp, 57000, Kuala Lumpur

Abstract: The initial goal of this work was to synthesize polypyrrole nanoparticles (PPy NPs) and PFFs nanocomposite as sensing material, placed on a screen-printed carbon electrode (SPCE) and used as aptasensor in detecting dimethyl methylphosphonate (DMMP). The aptasensor constructed after the optimization of sonication of PPy NPs and PFFs were optimized in two ways: aptamer concentration and incubation periods. Electrochemical measurement involving cyclic voltammetry (CV) analysis attested the improvement concerning the sensitivity of the modified SPCE using PPy NPs and PFFs and the selectivity thereof using different analytes including DMMP were determined using differential pulse voltammetry (DPV). The PPy NPs and PFF both showed significant decrease in the oxidation peak current with the presence various concentration of DMMP and various incubated duration, signifying the sensitivity of the modified SPCE.

Keywords: cyclic voltammetry, aptasensor, nanocomposites, different pulse voltammetry

Introduction

Electrochemical detection is based on a redox interaction between immobilized biomolecules or a detectable electrical current formed by chemical species on a working electrode and the target analyte [1]. Since the bio-electrochemical components that make up this sensor typically function as transduction elements, biological reactions can either result in charge accumulation that can be measured using amperometric, conductometric, potentiometric techniques or signal change that is capable of being utilized to measure impedance, conductance or measurable current [2]. Figure 1 illustrates the interactions that take place when bio-receptors like enzymes, antibodies, DNA, and aptamer are immobilized with biosensing layers such as nanoparticles, graphene or carbon nanotubes, which are capable of converting data from relevant transducer elements into quantifiable electrical properties like as current or voltage [3].

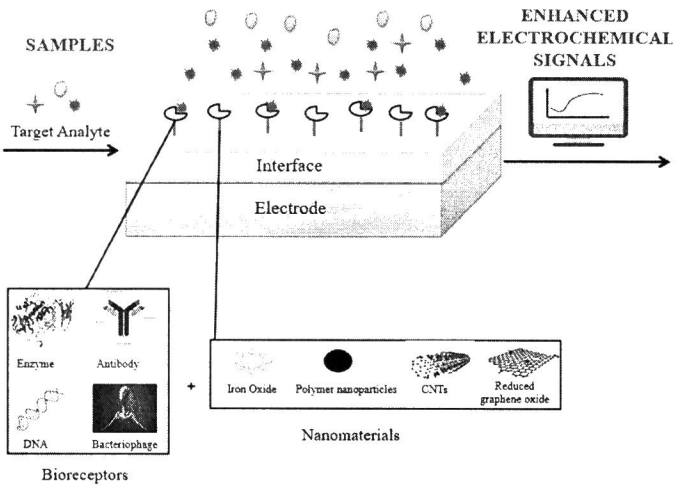

Figure 1. Electrochemical biosensor.

Electrochemical analysis of the PPy NPs and PFFs nanocomposite was performed using cyclic voltammetry (CV) and differential pulse voltammetry (DPV) techniques. CV is a simple technique for measuring the formal potential of half-reactions in which both the oxidized and reduced forms are stable for the time required to construct a current-potential graph, also known as a voltammogram while a differential method that monitors the development of a peak for a particular redox process is DPV [4,5]. For the detection of the analyte DMMP (10 µL), the test electrode is a screen-printed carbon electrode (SPCE) containing polypyrrole nanoparticles (PPy NPs) and polypyrrole-iron oxyhydroxide (PFFs) nanocomposite. SPCEs are commonly used as sensor constructs because they are easy to use and affordable to produce [6]. The redox analyte ferricyanide $[Fe(CN)_6]^{-3}$ is used to detect the electron transfer process, which evaluates the performance of the modified electrode [7].

Materials and Methods

Materials: Polypyrrole nanoparticles (PPy NPs) were made using pyrrole monomer as a starting material. Iron (III) oxide was then added to PPy NPs to create polypyrrole-iron oxyhydroxide (PFFs). As the primary components, PPy NPs, PFFs and aptamer were selected. These substances were employed to alter the screen-printed carbon electrode's (SPCE) surface in order to improve the sensor's sensitivity and selectivity.

Polymerization of PPy NPs: To stabilize the creation of nanoparticles, 40 wt% of sodium dodecylbenzenesulfonate (SDBS) surfactant was magnetically spun in 40 mL of distilled water at room temperature. The surfactant solution was then added dropwise with 19 wt% and 14.9 mmol of pyrrole monomer followed by 41 wt% ferric chloride (FeCl3) as an oxidant dissolved in distilled water. For two hours, the chemical polymerization was allowed to proceed at ambient temperature. In order to improve the dispersion of nanoparticles, a sonication method was applied in the manufacture of PPy NPs. Prior to washing the solution with excessive methyl alcohol, the solution was sonicated at various sonication durations to evaluate the impact of sonication on the generation of PPy NPs [8].

Fabrication of PFFs Nanocomposites

Using the same method, polypyrrole nanoparticles-iron oxyhydroxide (PFFs) were created utilizing the generated PPy NPs and then mixed for two hours with 10 wt% $FeCl_3$ in two different beakers. The combinations were then added to sodium hydroxide (NaOH) solutions at 1.9 and 3.7 wt%, and mixed for an hour. Then, these mixtures were split into two separate $FeCl_3$ weight percentages (5 wt% and 10 wt%). Each mixture was magnetically swirled for two hours to make sure all its components were thoroughly combined, then sonicated for an hour at room temperature. The precipitate was then dried in a vacuum oven for 12 hours at 60 °C after being rinsed numerous times with ethanol [8].

Electrochemical measurement: The PPy NPs and PFFs were all dissolved in 0.005 L of methanol and drop-cast on top of a screen-printed carbon electrode (SPCE) in an amount of 0.005 g. For the sensor preparation, the SPCE was washed with 1 mL distilled water, dried for one minute, dropped 10 µL of PPy NPs or PFFs, washed again with 1 mL of distilled water, dried again for one minute before dropped 100 µL of 5 mmol ferricyanide ($[Fe(CN)_6]^{3-}$) in 0.1 M of KCl solution prior to CV analysis and the scan rate was kept constant at 50 mVs^{-1} for eight cycles in order to obtain the highest oxidation peak current.

Modified aptasensor: Before being prepared in various concentrations and repeatedly incubated on top of SPCE modified PPy NPs (0.005 g) and PFFs (0.005 g) nanocomposites, the aptamer was initially diluted to a concentration of 100 µM in 1.292 mL of phosphate buffer saline (PBS) solution. This allowed the determination of the best concentration and incubation times for detecting the target analytes in this study [DMMP, methanol, acetonitrile, hexane, and dichloromethane (DCM]. In this sensor device, the AuNPs served as a linker between the sensor surface and the thiol aptamer.

Results & Discussions

Optimal starting sensing materials:

Bare electrodes, PPy NPs with one and three hours sonication periods and PFFs (5 and 10 wt%) in 5 mmol of $[Fe(CN)_6]^{-3}$ in 0.1 M of KCl solution were analyzed using CV voltammogram (Figure 2). Table 1 pointed out that the oxidation peak current for the bare SPCE was generated with a peak separation, ΔE_p of 240 mV at a current of 57.24 µA. While PPy NPs sonicated for three hours provided 73 µA of oxidation peak current with ΔE_p of 186mV, the SPCE treated with PPy NPs after one hour of sonication showed an increase in oxidation peak current of 77.76 µA with ΔE_p of 178 mV. Due to the PPy NPs finer particle size, which increases current transfer, one-hour sonicated PPy NPs produced a little larger current than three-hour sonicated PPy NPs. While the reduction of oxidation peak currents in the SPCE with PFFs containing 5 and 10 wt% were 70.07 µA (ΔE_p of 166 mV) and 69.16 µA (ΔE_p of 190 mV), respectively.

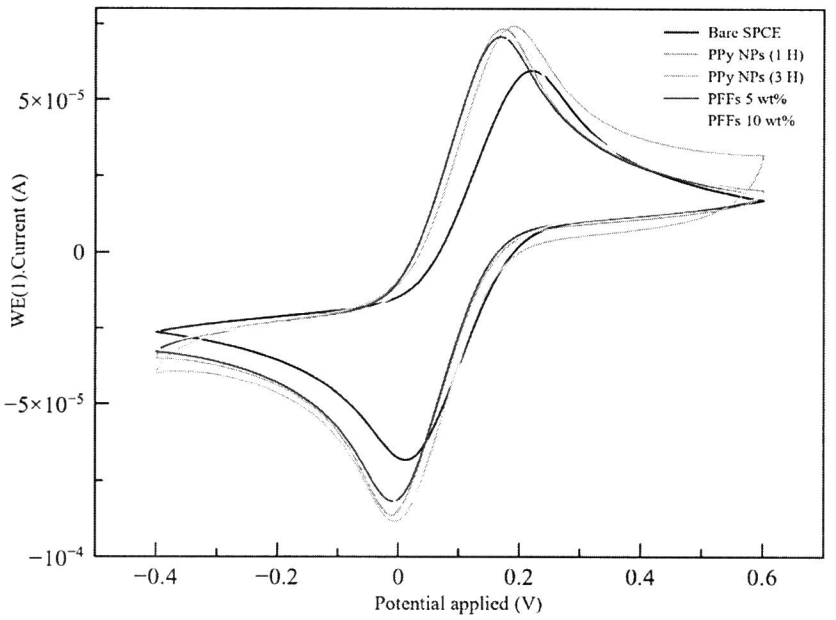

Figure 2. Cyclic Voltammogram.

Table 1. CV Data Collections

Sensor system	Oxidation peak current (μA)	Peak separation, ΔE_p (mV)	Percentage of current increase (%)
Bare SPCE	57.24	240	None
PPy NPs (1 H)	77.76	178	36
PPy NPs (3 H)	73	186	28
5 wt% PFFs	70.07	166	22
10 wt% PFFs	69.16	190	20

Figure 3 demonstrates that the increase in surface area enhanced the current signal of one-hour sonicated PPy NPs by up to 36%, surpassing that of three-hour sonicated PPy NPs (28%), 5 wt% PFFs by 22%, and 10 wt% PFFs by 20%. The decrease in oxidation peak current for the PFFs nanocomposite for both 5 and 10 wt% appeared to be related to the presence of FeOOH molecules with relatively high resistance [9]. These findings were equivalent to those of prior papers that reported on FESEM and TEM analyses [8]. Additionally, it appeared that the SPCE modified with PPy NPs (ΔE_p of 178 mV) had lower peak separation values than the bare electrode (ΔE_p of 240 mV) and the other modified electrodes because of an increase in the contact surface area between the PPy nanostructure and the electrolyte $[Fe(CN)_6]^{-3}$.

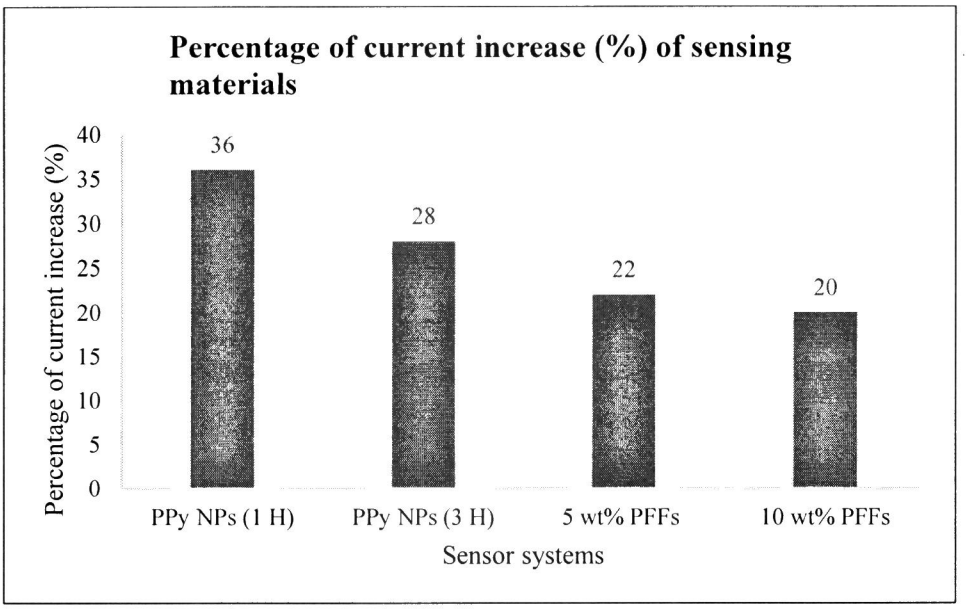

Figure 3. Bar graph of percentage peak current increase.

Optimal sensitivity of sensor modified PPy NPs:

One-hour sonicated PPy NPs and 5 wt% PFFs were chosen as the best sensing materials to modify on top of SPCE. The oxidation peak of voltage in DPV is estimated by data acquired from a preceding CV voltammogram, which is between -0.30 V and 0.60 V. The DPV mode was chosen because the peaks are sharper and more defined at lower analyte concentrations than the CV mode [10]. The DPV analysis was carried out on 10 μL of one-hour sonicated PPy NPs in the presence of various concentrations of dimethyl methylphosphonate (DMMP) analyte (1000 ppm, 250 ppm, 1 ppm, 100 ppb, 1 ppb, 0.1 ppb, and 0.01 ppb). Figure 4 depicts the DPV voltammogram of PPY NPs with varying DMMP concentrations. The oxidation peak current increased as the concentration of DMMP decreased. However, when DMMP analyte was present, the oxidation peak current decreased as compared to the bare SPCE. Figure 5 clearly shows the proportion of current decline. By introducing 1000 ppm analyte, the percentage of oxidation peak current was lowered to 35.5 %, and it was further reduced to 2.93 % at 0.1 ppb DMMP analyte. At the lowest DMMP concentration (0.01 ppb), there was only a small current drop of 0.22 %.

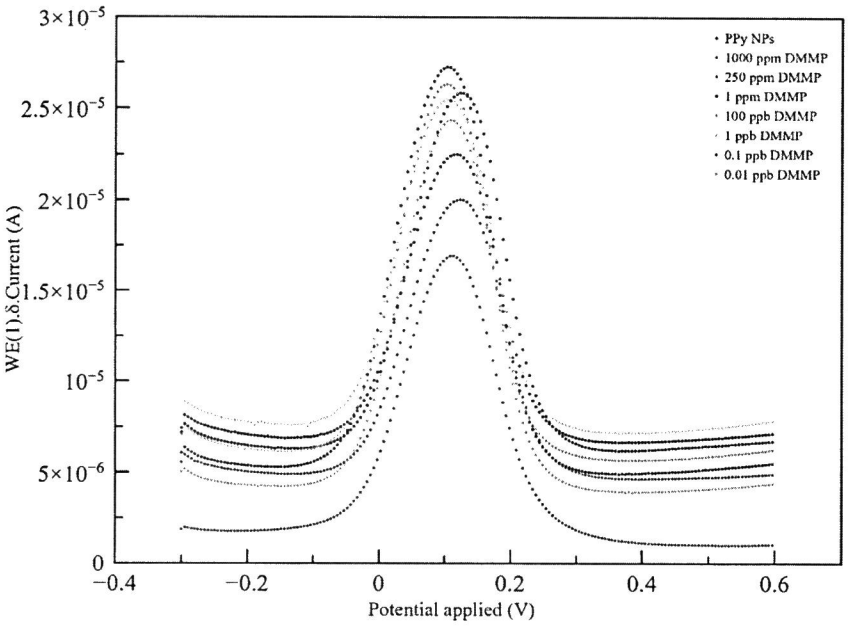

Figure 4. DPV Voltammogram of PPy NPs.

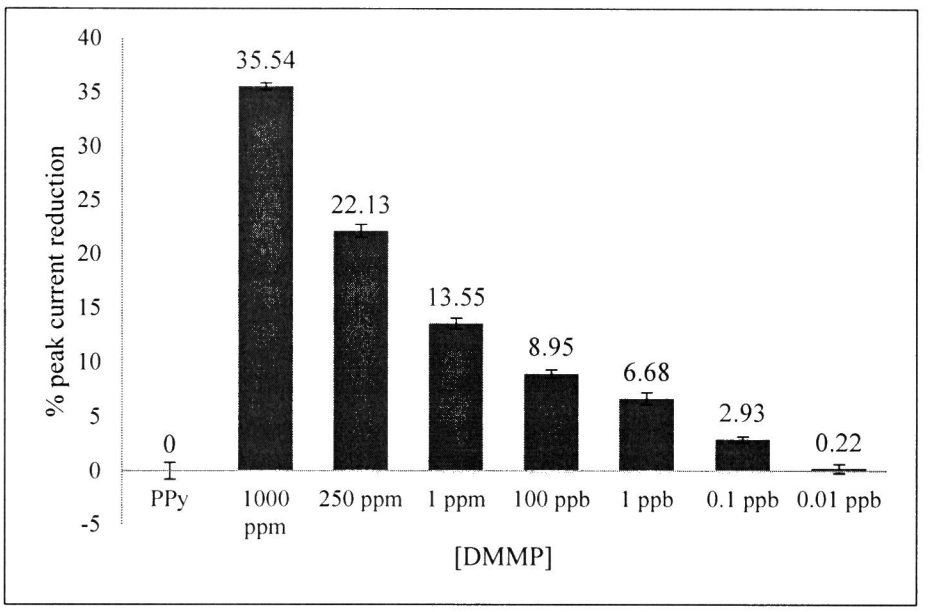

Figure 5. Percentage current reduction bar graph.

The quantity of doping in polymers such as PPy NPs had a significant impact on their conductivity. As a result, electron interactions between PPy NPs and DMMP could significantly alter the polymer doping levels. The adoption of an electron-donor substance as the sensing analyte may have reduced the PPy NPs current [11]. When PPy interacts with DMMP, a highly strong electron donor, the concentration of charge carriers (electron holes) drops along the PPy NPs chain. As the interactions between PPy NPs and DMMP increased, the resistivity of the PPy rose, lowering the oxidation peak current appropriately [12]. Figure 6 represents a calibration curve derived from the DPV analysis and used to establish the limit of detection (LOD) of DMMP. The graph shows a linear regression line with an R^2 value of 0.8996 [13]. The LOD determined by the calibration curve is 3.58 ppm, but the accuracy was not sufficiently substantial because the oxidation peak can still be observed at lower concentrations as low as 0.1 ppb.

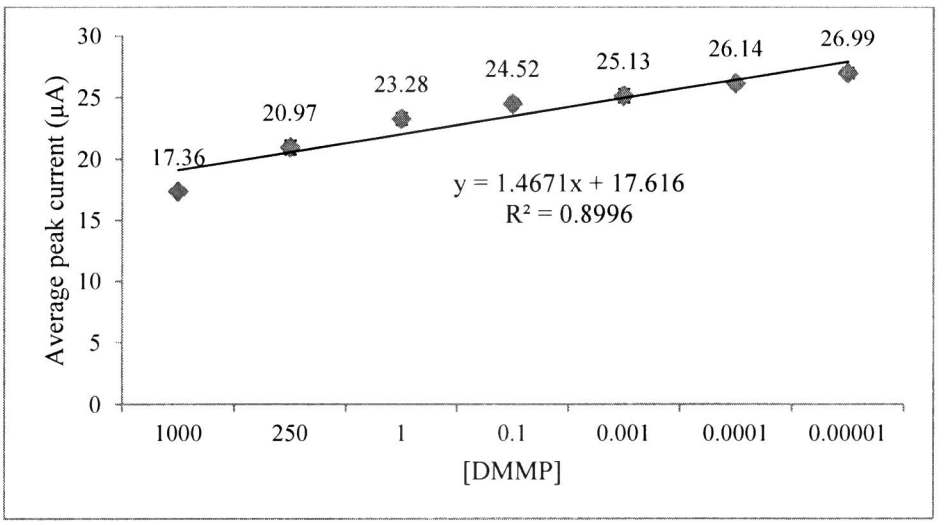

Figure 6. Calibration curve graph.

Optimal sensitivity of sensor modified PFFs:

Figure 7 displays the PFFs system's DPV. Figure 8 shows the percentage of oxidation peak current reduction. With a DMMP concentration of 1 ppb, the PFFs sensors revealed a progressive decrease in percentage peak current drop. The percentage peak current did not decrease at 0.1 and 0.01 ppb DMMP concentrations, and the current began to grow. The interaction of DMMP and iron oxyhydroxide (FeOOH) in PFFs nanocomposite was bonded by hydrogen bonding between the P=O groups of DMMP and the -OH in FeOOH (Figure 9).

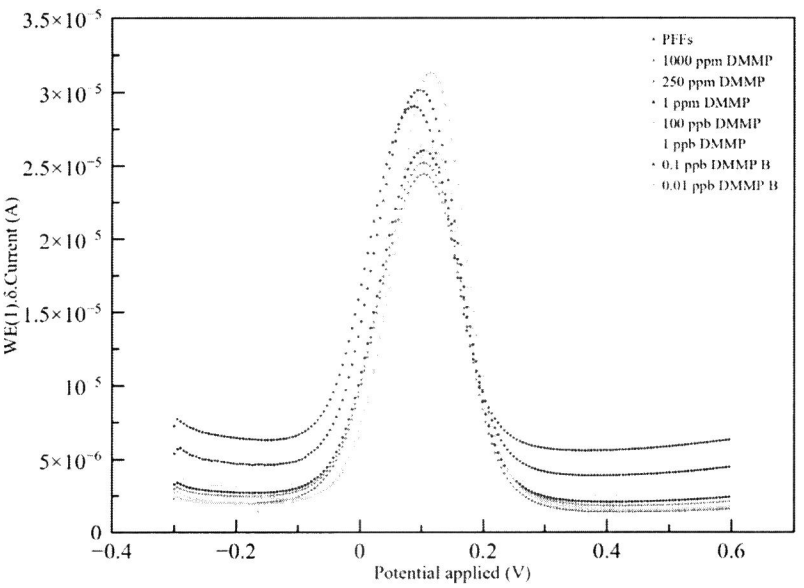

Figure 7. DPV graph.

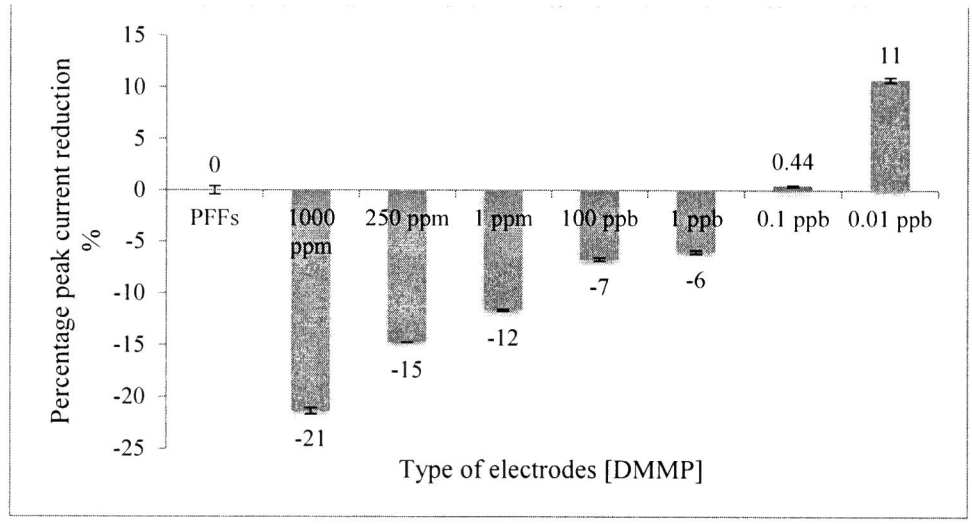

Figure 8. Percentage current reduction graph.

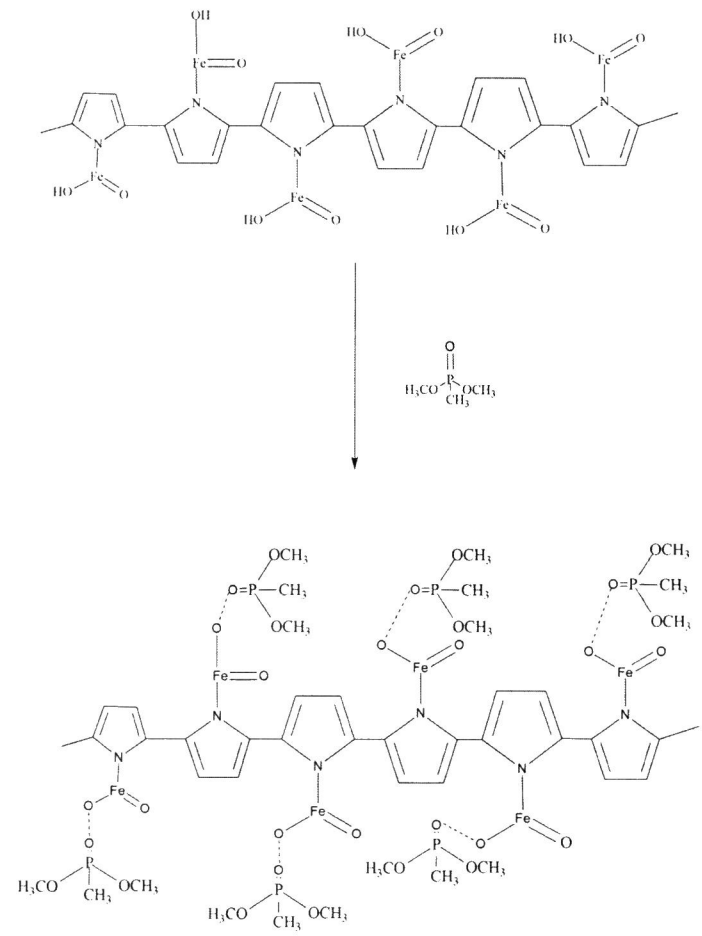

Figure 9. PFFs interaction with DMMP.

This phenomenon occurs due to the FeOOH particles accumulated as a result of unevenly stacked PFFs created during the fabrication process, interrupting the electron transfer channel and resulting in shrinkage of the nucleate site of FeOOH in PFFs, making it less sensitive in detecting lower concentrations of DMMP [14]. The graph indicates a linear regression line with an R^2 value of 0.9484 (Figure 10). The gradient value was used to determine LOD, which was found to be 5.802 ppm, slightly higher than the PPy NPs system (3.58 ppm). This state is

caused by an increase in surface area, as shown by TEM research, because the size of PFFs is bigger than that of PPy NPs, resulting in a reduction in sensing active sites [8].

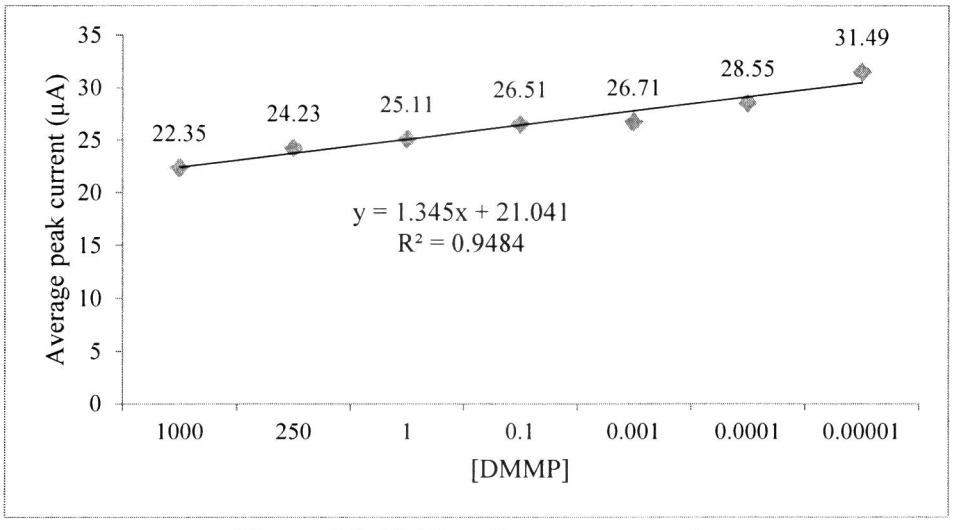

Figure 10. Calibration curve graph.

Optimization of aptasensor modified PPy NPs & PFFs (Concentration of aptamer):
Polypyrrole nanoparticles (PPy NPs) and polypyrrole-iron oxyhydroxide nanocomposite (PFFs) were used as immobilization materials on the screen-printed carbon electrode (SPCE) to improve sensitivity [15]. The use of gold nanoparticles (AuNPs) as aptamer immobilization support in aptasensor production is also well known, and this is critical for binding the thiol-based aptamer [16]. The aptamer was expected to particularly capture the DMMP and drive the sensing material to be more selective. The aptamer concentration (1 to μ5M) was explored to improve the detection performance of the PPy NPs and PFFs based aptasensor. Although the aptamer was predicted to trap the DMMP, the aptamer concentration might alter the amount of DMMP bound and the electrochemical response of the aptasensor.

Figure 11 depicts the DPV voltammogram of a PPy NPs/aptamer system cultured for one hour with and without 1 ppm DMMP. Without the presence of DMMP, the peak of oxidation current was reduced by only 3 to 16%, however the modified SPCE (with the presence of DMMP) reduced the peak of oxidation current by 27 to 40% for aptamer concentrations ranging from 1 to μ5 M. The oxidation peak current was lowered by up to 16% at the maximum aptamer concentration (5 μM). According to this scenario, the aptamer successfully bound on the top of the AuNP surface via the thiol end group of aptamers [17]. The addition of DMMP significantly impacted the oxidation peak current. The intensity of the oxidation peak current was greatly lowered (by 27 to 40% of the current reduction). The addition of 1 μM of aptamer concentration results in the greatest current reduction (40%). These new findings validated the ability of aptamer to trap DMMP and so corroborated the hypothesis previously reported by Zhao et al. in detecting DMMP utilizing a cantilever-based aptasensor for detecting nerve agent simulant DMMP at trace levels in aqueous matrices [18]. Figure 12 suggests the percentage of the current drop in each system.

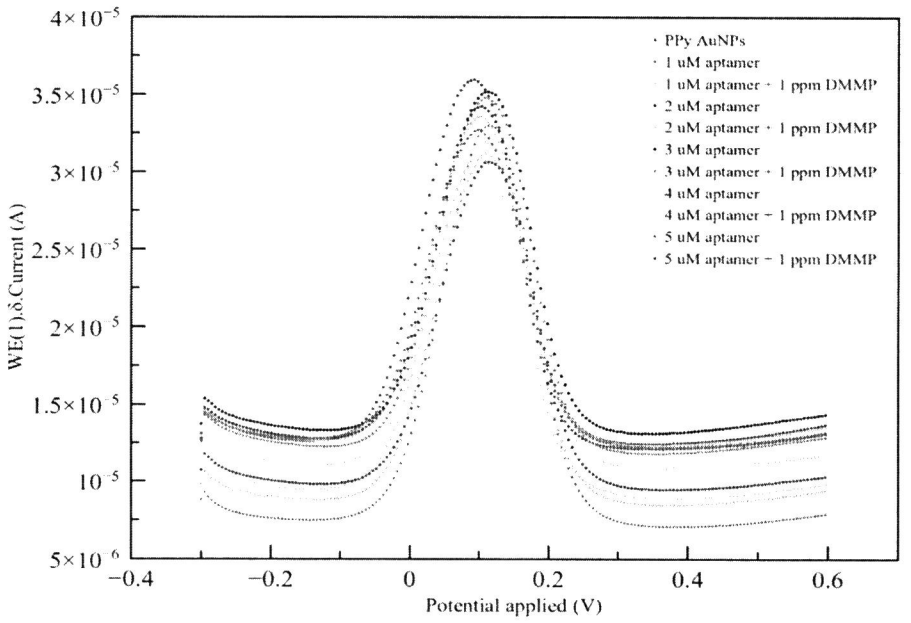

Figure 11. DPV of PPy NPs/aptamer.

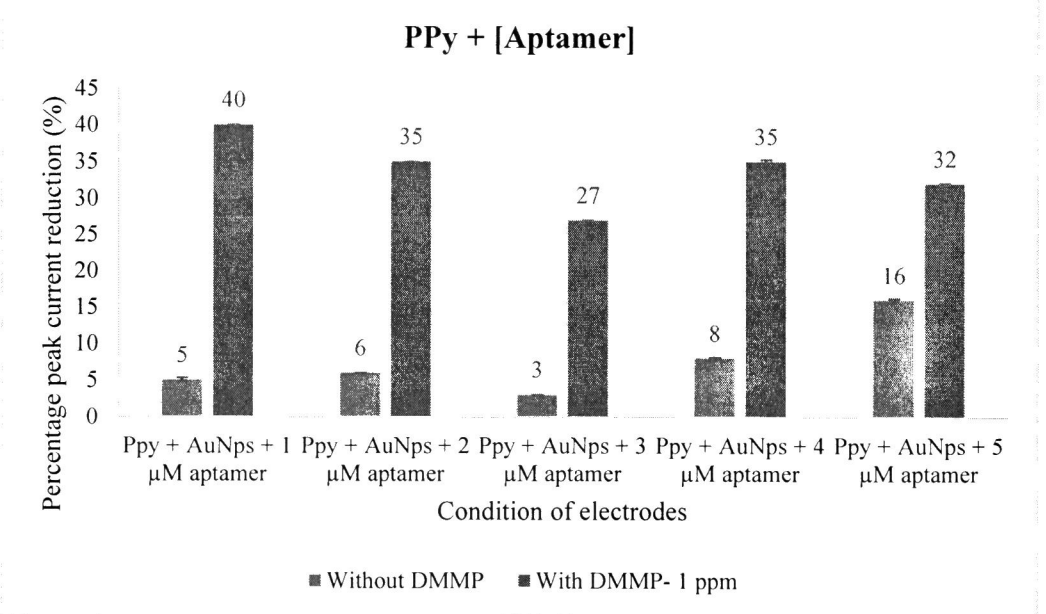

Figure 12. Bar graph for percentage current reduction.

Figure 13 represents a DPV voltammogram of PFFs/aptamer systems with and without 1 ppm DMMP. Without the addition of DMMP, the peak of oxidation current decreased from 4 to 15% for aptamer concentrations of 1 to 5 μM incubated for one hour. At 4 μM of aptamer, the greatest current drop was recorded. The aptamer effectively bound on the top of the AuNP surface via the thiol end group of aptamers, which is equivalent to the PPy NPs system [17].

The addition of the DMMP may potentially cause a significant change in oxidation peak current. The intensity of the oxidation peak current was greatly lowered (from 26 to 49%) of the current reduction. At 5 μM aptamer concentration, the highest current reduction (49%) was observed. In comparison to the PPy NPs system, 40% current reduction was obtained at 1 μM of aptamer, whereas the PFFs system required the addition of 3 μM of aptamer to obtain 42%

current reduction. The phenomenon suggested that the PPy NPs system only needed a modest amount of aptamer to achieve the greatest current decrease. Figure 14 clearly shows the percentage of current reduction in each system.

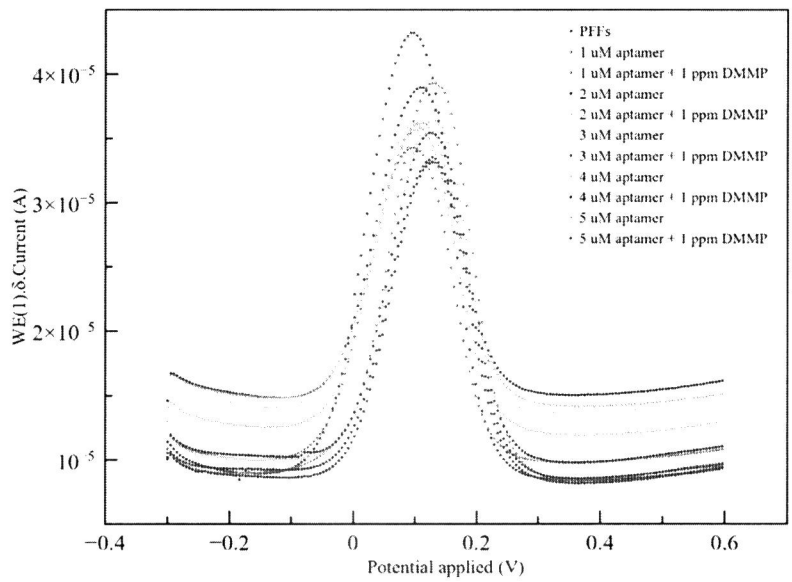

Figure 13. DPV of PFFs/aptamer.

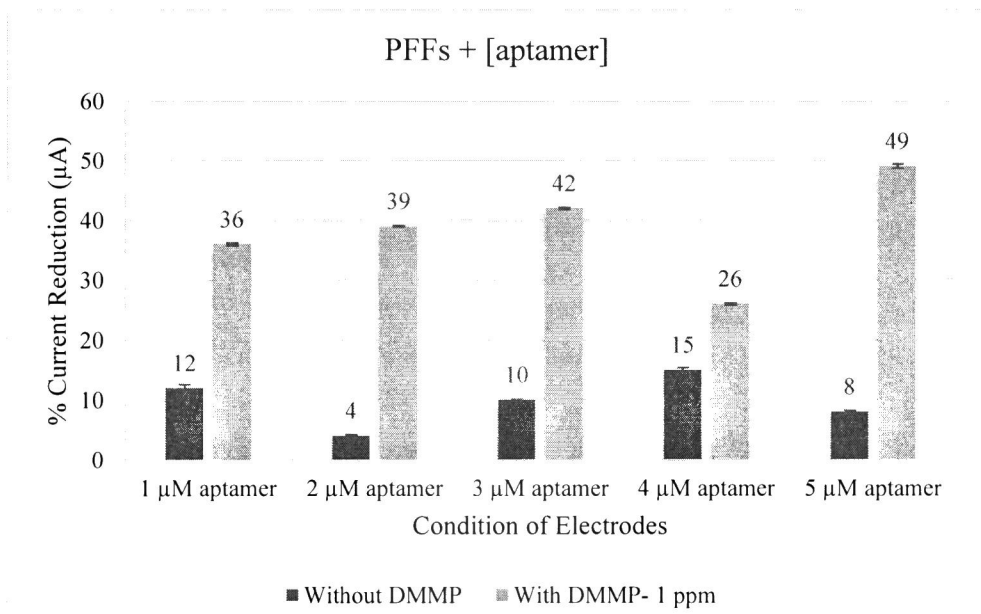

Figure 14. Bar graph for percentage current reduction

Optimization of aptasensor modified PPy NPs & PFFs (Incubation time of aptamer):
During the incubation phase, the aptamer incubation period revealed as a significant factor determining sensor performance. If the incubation time is too short or takes too long, the aptamer cannot be properly altered on the electrode surface. In order to suppress the remaining active sites on the electrode surface and avoid non-specific binding, the incubation time is also critical [19]. The aptamer incubation length was changed in this study from 1 hour to 28 hours (1, 4, 20, 24, and 28 h).

In optimizing the aptamer incubation duration for the PPy NPs system, 1 μM of aptamer was chosen since it gave the maximum oxidation peak reduction in the presence of 1 ppm DMMP. Figure 15 depicts the DPV voltammogram for this system. The oxidation peak current appears to grow as the incubation duration increases. After 1 hour of incubation, the lowest oxidation peak current was obtained. Figure 16 shows a bar graph illustrating the percentage of current reduction, which may be utilized to clearly observe the influence of aptamer incubation duration.

The results showed that incubating the aptamer on the top of the electrode for 1 hour was significantly more effective. The percentage current reduction was greatest when the incubation period approached 1 hour, which could be attributed to the aptamer's saturation target binding amount. As a result, the optimal incubation period was determined to be one hour. Yang et al. (2020) discovered a comparable result for their label-free detection of oxytetracycline in milk samples using an electrochemical aptasensor based on a diazonium-coupling reaction [20].

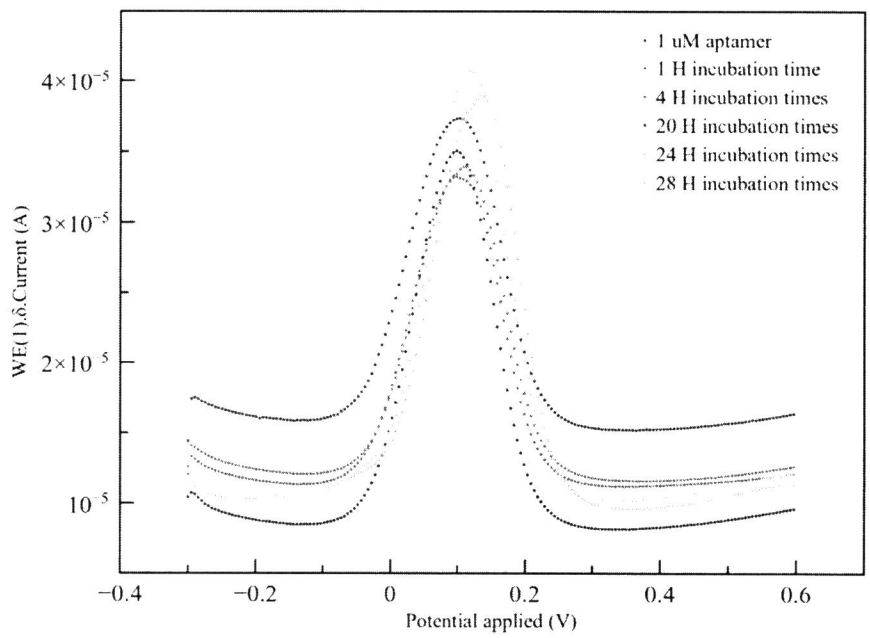

Figure 15. DPV of PPy NPs/aptamer

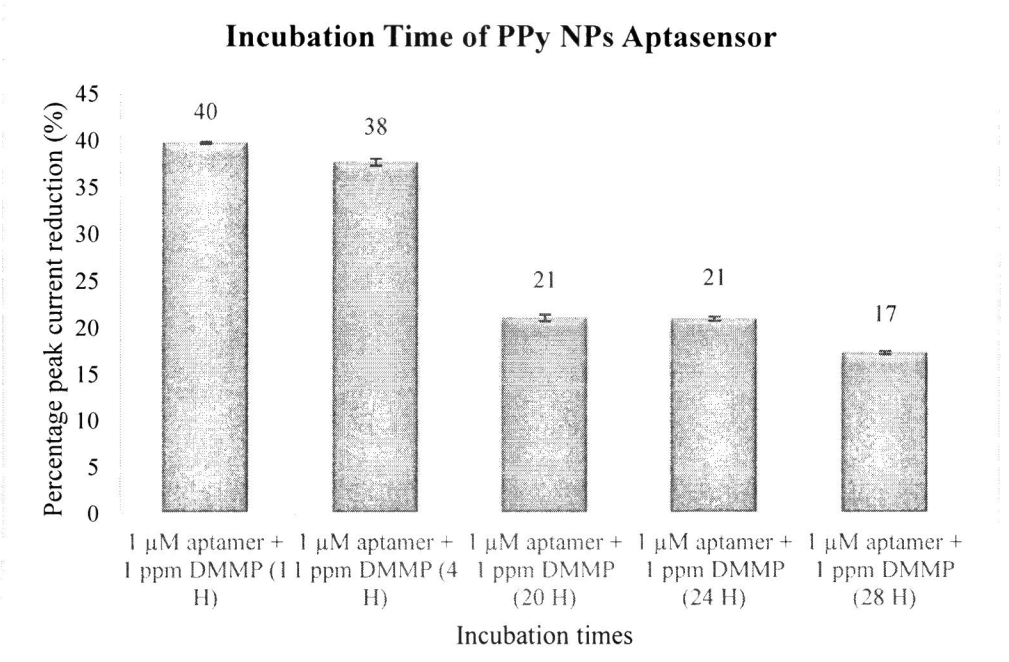

Figure 16. Bar graph for percentage current reduction

In order to optimize the aptamer incubation duration for the PFFs system, 5 µM of aptamer was chosen because the system provided the largest peak current reduction of 49% in the presence of 1 ppm DMMP. Figure 17 conveys the DPV voltammogram for this system. Unlike the PPy NPs system, the PFFs system did not show a distinct trend. The peak oxidation peak current at 1, 4, and 20 hours was nearly identical with only a minor change. The lowest oxidation peak current was measured after 1 hour of incubation.

Figure 18 shows the percentage of current decline. The results showed that 1 hour of incubation time was significantly better than 2 hours in incubating the aptamer on top of the electrode. Furthermore, aptamer incubation times of 24 and 28 hours show a very modest percentage of current reduction, implying that partial aptamer hybridization occurs [21]. While 4 and 20 hours provided equivalent reduction currents, the 1-hour incubation time was chosen as the ideal duration because it could significantly cut the time incubation effectively and overall minimize the time necessary for electrode preparation.

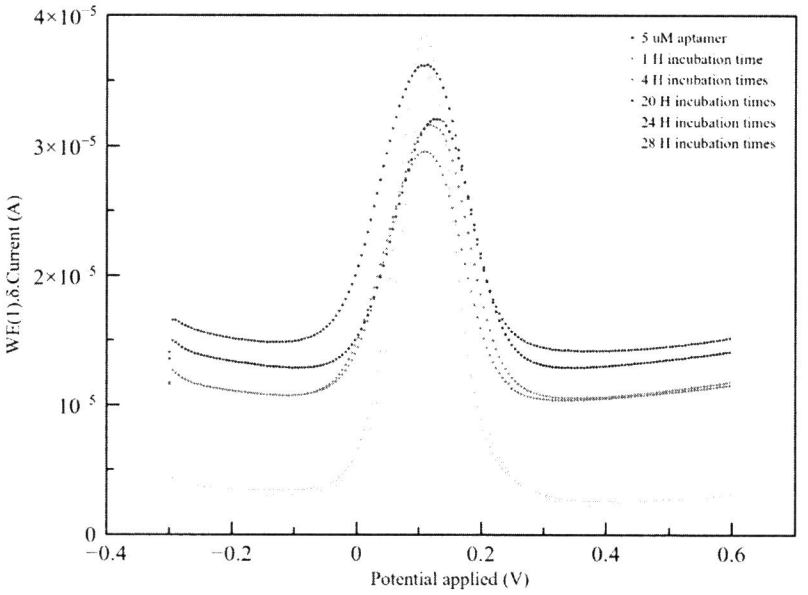

Figure 17. DPV of PFFs/aptamer.

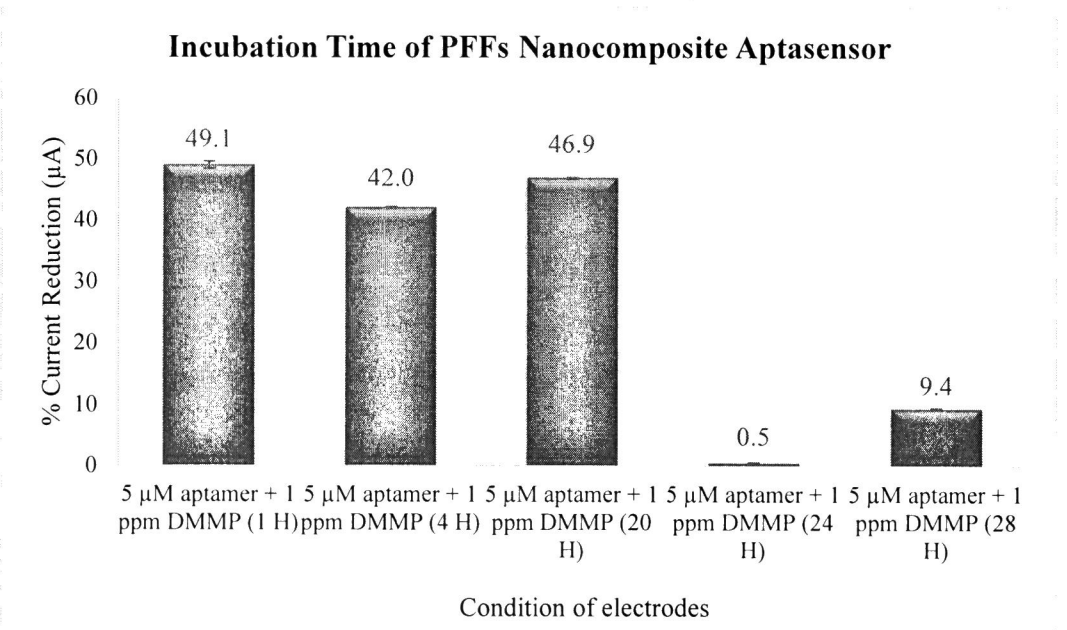

Figure 18. Bar graph for percentage current reduction.

Optimization selectivity of aptasensor modified PPy NPs:

In this study, aptamer was used as a biological recognition molecule that was specifically sequenced in recognizing DMMP. To validate the selectivity of the proposed aptasensor, different analytes such as methanol, hexane, dichloromethane (DCM) and acetonitrile were examined. In order to evaluate the sensor's selectivity, four types of sensor systems were created: PPy NPs sensor, PFFs composite sensor, PPy NPs aptasensor and PFFs composite aptasensor in the presence of 1 ppm DMMP and other analytes.

The DPV voltammogram of a PPy NPs-based sensor is shown in Figure 19. It can be noticed that the oxidation peak current of DMMP and hexane decreased, whereas the peak current of

DCM, Acetonitrile, and methanol increased. Although this method could detect hexane, the percentage of peak reduction was only 6%, which was significantly lower than the 41% decrease of the oxidation peak in the presence of DMMP. Figure 20 clearly shows the percentages of peak reduction.

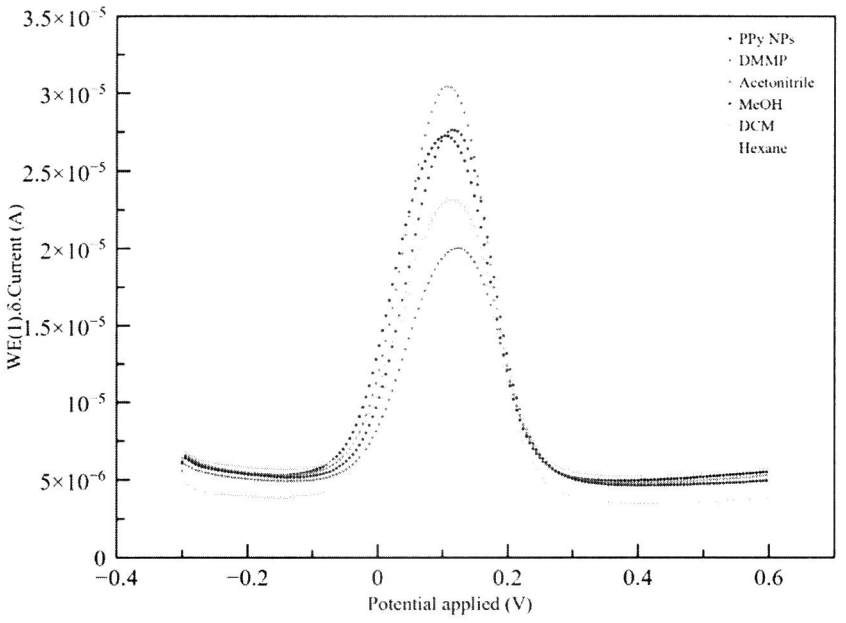

Figure 19. DPV of PPy NPs selectivity.

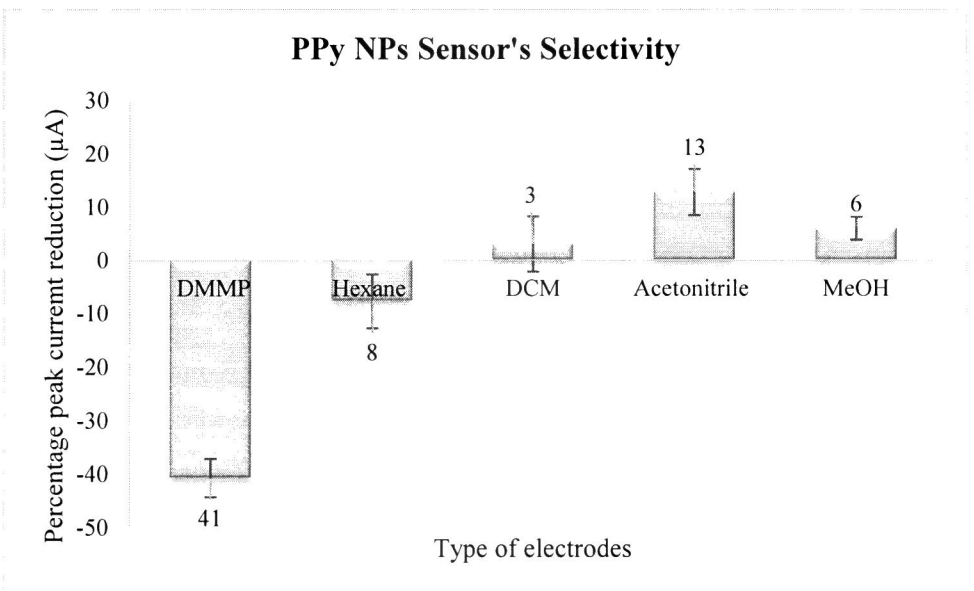

Figure 20. Bar graph of percentage current reduction.

In contrast, the lowering of the oxidation peak in the system of PPy NPs aptasensor (with the presence of 1 uM aptamer) could only be observed in the presence of DMMP, as demonstrated in the DPV voltammogram of PFFs based aptasensor in Figure 21. The oxidation peak current of the other analyte increased. The current reduction percentage was also substantial, at 40%. Figure 22 depicts a bar graph depicting the percentage of peak current reduction for the PPy

NPs aptasensor system. According to the bar graph, using the PPy NPs aptasensor to detect the analyte resulted in a very high current rise (> 26%).

This discovery revealed that the aptamer effectively increased the aptasensor's selectivity, as only DMMP shows a high current reduction (40%). The aptasensor's great selectivity was attributed to the aptamer's specific identification ability, which could selectively detect and capture the target DMMP with self-conformation alteration [20].

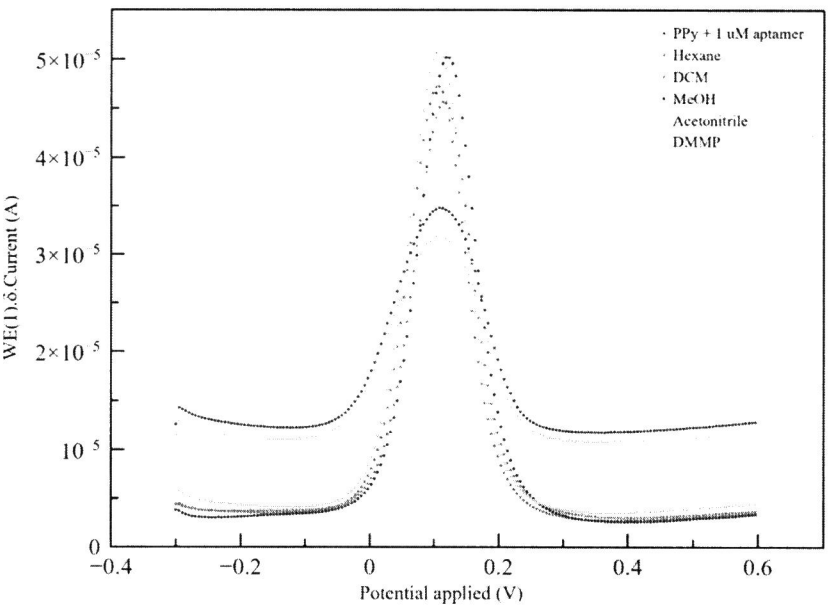

Figure 21. DPV of PPy NPs aptasensor selectivity.

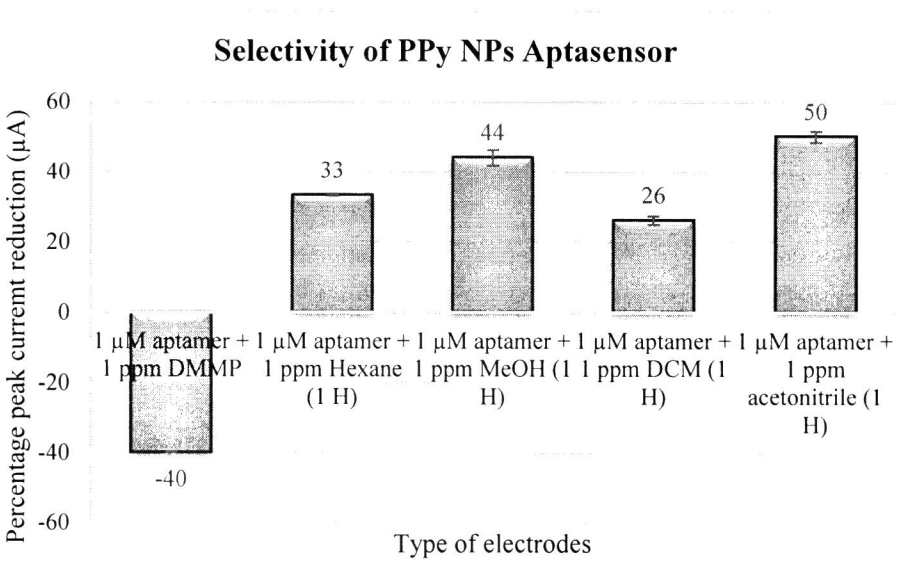

Figure 22. Bar graph of percentage current reduction.

Optimization selectivity of aptasensor modified PFFs:

The identical analyte was utilized to validate the sensor's performance for the PFFs composite-based sensor. Figure 23 shows the DPV voltammogram of a PFFs sensor system. According to Figure 24, the oxidation peak was reduced in three analytes, namely DMMP, hexane, and acetonitrile. However, when compared to methanol and hexane, the DMMP provided the

largest decrease peak. The oxidation peak current rose in methanol and DCM in a manner comparable to the PPy NPs system. This event revealed that the PFFs sensor might detect acetonitrile and hexane in addition to DMMP. Nonetheless, the present reduction percentage was lower than DMMP, with 8 and 26% compared to 56%.

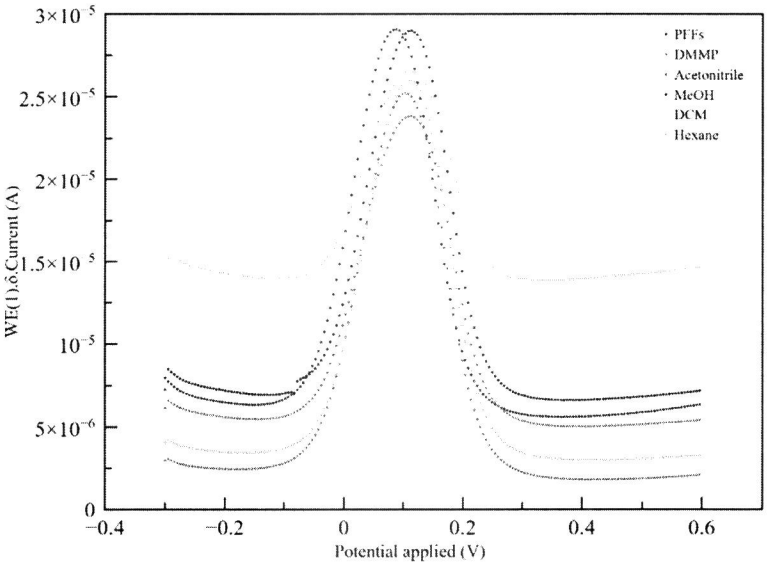

Figure 23. DPV of PFFs selectivity.

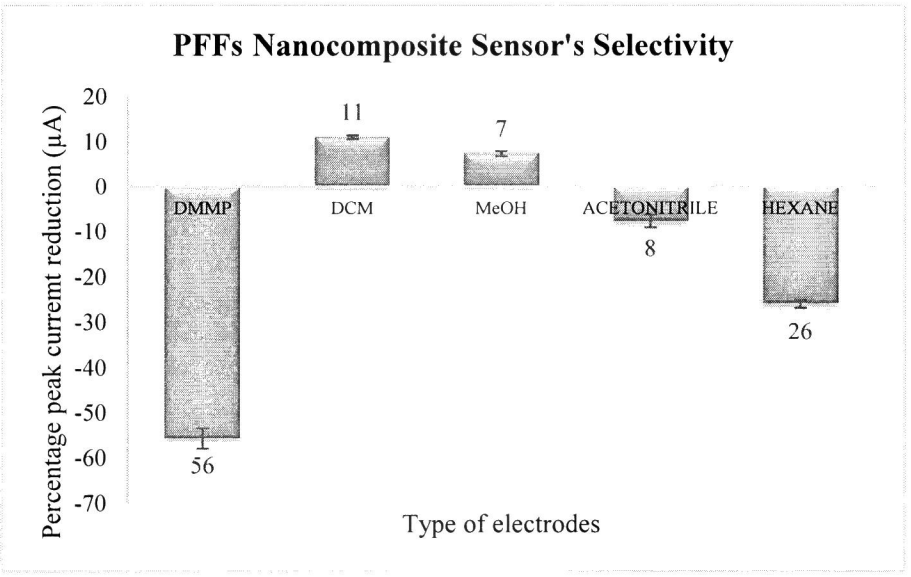

Figure 24. Bar graph of percentage current reduction.

Furthermore, the presence of aptamer in PFFs aptasensor produced a significant improvement. According to the DPV voltammogram, only DMMP provided the reduction in oxidation peak current. The oxidation peak current of the other analyte increased in a positive manner. Figure 25 depicts the DPV voltammogram of the PFFs aptasensor system. According to the percentage of peak current reduction shown in Figure 26, the DMMP analyte showed a 49% reduction in peak current, whereas the other analytes showed a positive increment ranging from 27 to 48%. The presence of aptamer in the PFFs aptasensor demonstrated the ability to selectively trap the DMMP. The high-selectivity PFFs aptasensor was related to a structural change in the aptamer

indicating that the target was recognized and associated with the aptamer, resulting in sensor current reduction via DPV [22].

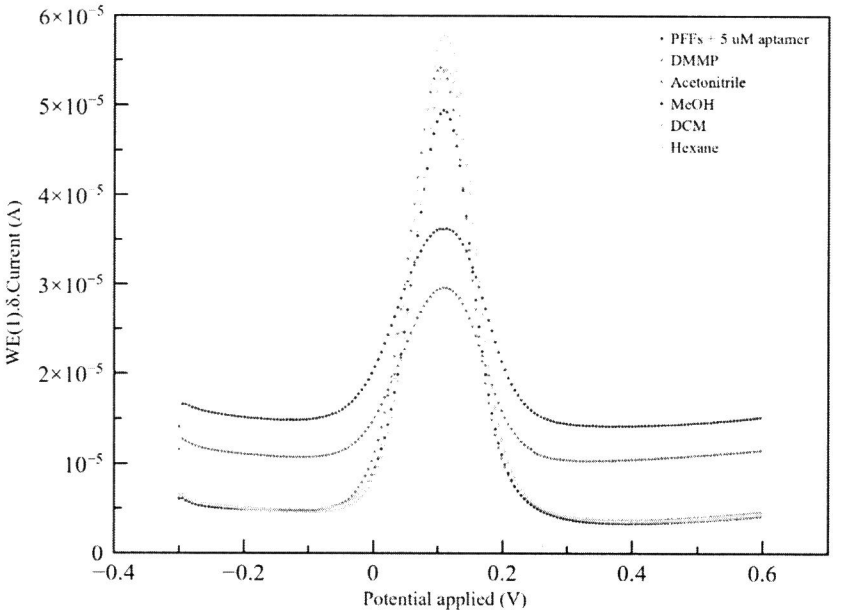

Figure 25. DPV of PFFs aptasensor selectivity.

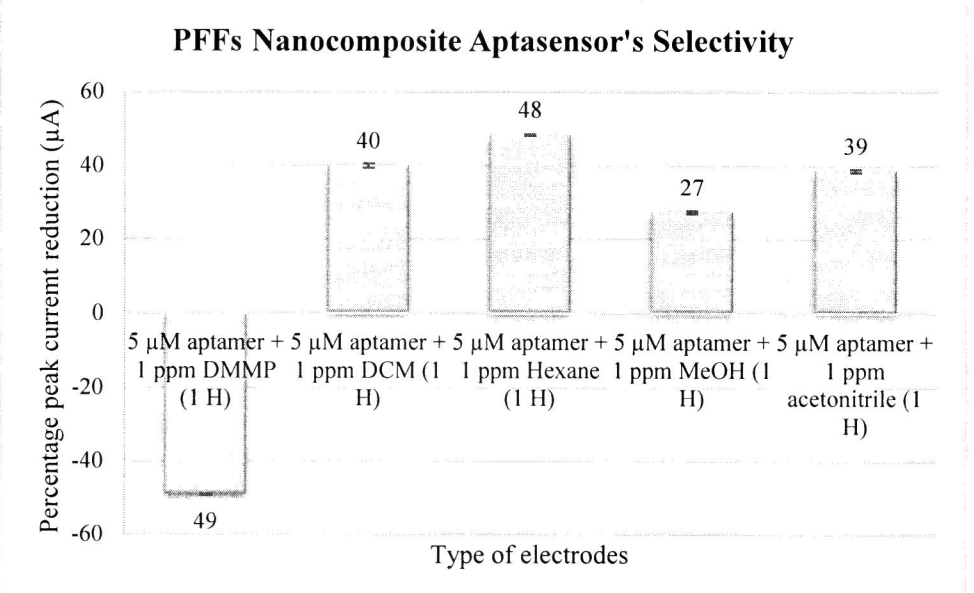

Figure 26. Bar graph of percentage current reduction.

Conclusion

Using cyclic voltammetry (CV), the optimal sensing materials for the electrochemical inquiry were determined as one hour sonication of PPy NPs (36%) and 5 wt% of PFFs (22%) nanocomposites. The first goal was to determine the effectively produced PPy NPs and PFFs nanocomposite as sensing materials. The aptasensor PPy NPs and PFFs are optimized under two conditions: aptamer concentration and incubation times. 1 μM of aptamer incubated for 1 hour is optimal for the PPy NPs aptasensor, while 5 μM of aptamer incubated for the same hour time is optimal for the PFFs aptasensor. The sensitivity and selectivity of new electrochemical sensors based on aptamer functionalized PPy NPs and PFFs were also studied.

The PPy NPs sensor is more sensitive and has a lower LOD of 3.576 ppm than the PFFs nanocomposites sensor, which has a LOD of 5.802 ppm. The finer the particles the greater the electron transfers of the sensor, consequently directly increased the peak current.
Meanwhile, the presence of aptamer integration of PPy NPs and PFFs nanocomposites sensor boosted selectivity of the sensor towards the target analyte DMMP in the presence of other analytes (methanol, DCM, acetonitrile, and hexane).

Acknowledgement
The authors are grateful to the Ministry of Education Malaysia, Development Fund F0020 for funding via UPNM/2018/CHEMDEF/ST/5.

References

[1] Abdul Rashid, J. I., Abdullah, J., Yusof, N. A. & Hajian, R. 2013. The Development of Silicon Nanowire as Sensing Material and Its Applications. Journal of Nanomaterials, 2013, 328093.
[2] Mishra, G. K., Barfidokht, A., Tehrani, F. & Mishra, R. K. 2018. Food Safety Analysis Using Electrochemical Biosensors. Foods, 7, 141.
[3] Rathee, K., Dhull, V., Dhull, R. & Singh, S. 2016. Biosensors Based on Electrochemical Lactate Detection: A Comprehensive Review. Biochemistry and Biophysics Reports, 5, 35-54.
[4] Aoki, K. J. & Chen, J. 2018. Tips Of Voltammetry. Voltammetry, Vol 1, 1-91.
[5] Bounab, L., Iglesias, O., Pazos, M., Sanromán, M. Á. & Gonzalez-Romero, E. 2016. Effective Monitoring of The Electro-Fenton Degradation of Phenolic Derivatives by Differential Pulse Voltammetry on Multi-Walled-Carbon Nanotubes Modified Screen-Printed Carbon Electrodes. Applied Catalysis B: Environmental, 180, 544-550.
[6] Ye, Y. & Ju, H. 2005. Rapid Detection of Ssdna and Rna Using Multi-Walled Carbon Nanotubes Modified Screen-Printed Carbon Electrode. Biosensors And Bioelectronics, 21, 735-741.
[7] Ganesh, V. & Lakshminarayanan, V. 2010. Microemulsion Phase as A Medium For Electrodeposition Of Nickel And Electron-Transfer Study Of Ferrocyanide–Ferricyanide Redox System. Journal Of Colloid and Interface Science, 349, 300-306.
[8] Diauudin, F. N., Mohd Noor, S. A., Abdul Rashid, J. I., Feizal Knight, V., Wan Yunus, W. M. Z., Ong, K. K., Mohd Kasim, N. A., Taufik, S., Samsuri, A. & Shamsudin, I. J. 2020. Preparation And Characterisation of Polypyrrole-Iron Oxyhydroxide Nanocomposite as Sensing Material. Advances In Materials Science and Engineering, 8762969.
[9] Liang, W., Poon, R. & Zhitomirsky, I. 2019. Zn-Doped Feooh-Polypyrrole Electrodes for Supercapacitors. Materials Letters, 255, 126542.
[10] Rizk, M., Hendawy, H. A., Abou El-Alamin, M. M. & Moawad, M. I. 2015. Sensitive Anodic Voltammetric Determination of Methylergometrine Maleate in Bulk and Pharmaceutical Dosage Forms Using Differential Pulse Voltammetry. Journal of Electroanalytical Chemistry, 749, 53-61.
[11] Lakard, B., Carquigny, S., Segut, O., Patois, T. & Lakard, S. 2015. Gas Sensors Based on Electrodeposited Polymers. Metals, 5, 1371-1386.
[12] Park, S. J., Park, C. S. & Yoon, H. 2017. Chemo-Electrical Gas Sensors Based on Conducting Polymer Hybrids. Polymers, 9, 155.

[13] Rogulski, M. & Badyda, A. 2020. Investigation Of Low-Cost and Optical Particulate Matter Sensors for Ambient Monitoring. Atmosphere, 11, 1040.
[14] Lee, J. S., Shin, D. H., Jun, J. & Jang, J. 2013. Multidimensional Polypyrrole/Iron Oxyhydroxide Hybrid Nanoparticles for Chemical Nerve Gas Agent Sensing Application. Acs Nano, 7, 10139-10147.
[15] Cho, E. J., Lee, J.-W. & Ellington, A. D. 2009. Applications Of Aptamers as Sensors. Annual Review of Analytical Chemistry, 2, 241-264.
[16] Liu, J. & Lu, Y. 2004. Adenosine-Dependent Assembly of Aptazyme-Functionalized Gold Nanoparticles And Its Application as A Colorimetric Biosensor. Analytical Chemistry, 76, 1627-1632.
[17] Wang, J., Meng, W., Zheng, X., Liu, S. & Li, G. 2009. Combination Of Aptamer with Gold Nanoparticles For Electrochemical Signal Amplification: Application To Sensitive Detection Of Platelet-Derived Growth Factor. Biosensors And Bioelectronics, 24, 1598-1602.
[18] Zhao, R., Jia, D., Wen, Y. & Yu, X. 2017. Cantilever-Based Aptasensor for Trace Level Detection Of Nerve Agent Simulant in Aqueous Matrices. Sensors And Actuators B: Chemical, 238, 1231-1239.
[19] Upan, J., Youngvises, N., Tuantranont, A., Karuwan, C., Banet, P., Aubert, P.-H. & Jakmunee, J. 2021. A Simple Label-Free Electrochemical Sensor For Sensitive Detection of Alpha-Fetoprotein Based on Specific Aptamer Immobilized Platinum Nanoparticles/Carboxylated-Graphene Oxide. Scientific Reports, 11, 1-9.
[20] Yang, Y., Yan, W., Guo, Y., Wang, X., Zhang, F., Yu, L., Guo, C. & Fang, G. 2020. Sensitive and Selective Electrochemical Aptasensor Via Diazonium-Coupling Reaction For Label-Free Determination of Oxytetracycline in Milk Samples. Sensors And Actuators Reports, 2, 100009.
[21] Peng, H., Hui, Y., Ren, R., Wang, B., Song, S., He, Y. & Zhang, F. 2019. A Sensitive Electrochemical Aptasensor Based on Mb-Anchored Go for The Rapid Detection of Cronobacter Sakazakii. Journal Of Solid-State Electrochemistry, 23, 3391-3398
[22] Li, S., Liu, C., Yin, G., Zhang, Q., Luo, J. & Wu, N. 2017. Aptamer-Molecularly Imprinted Sensor Base on Electrogenerated Chemiluminescence Energy Transfer for Detection of Lincomycin. Biosensors And Bioelectronics, 91, 687-691.